Interesting Structural and Dynamical Behaviors Exhibited by the AF-6 PDZ Domain upon Bcr Peptide Binding†

Xiaogang Niu, Quan Chen, Jiahai Zhang, Weiqun Shen, Yunyu Shi, and Jihui Wu*

Hefei National Laboratory for Physical Sciences at Microscale, University of Science and Technology of China, and School of Life Sciences, University of Science and Technology of China, Hefei, Anhui 230026, People's Republic of China

Received July 3, 2007; Revised Manuscript Received October 29, 2007

ABSTRACT: PDZ (postsynaptic density-95, disks large, zonula occludens-1) domains are small, protein−protein interaction modules that have multiple binding surfaces for the docking of diverse molecules. These domains can propagate signals from ligand-binding site to distal regions of the structure through allosteric communication. Recent works have revealed that picosecond to nanosecond time scale dynamics play a potential role in propagating long-range signals within a protein. Comparison of AF-6 PDZ domain structures in free and complex forms shows a conformation rearrangement of distal surface 2, which is far from the peptide binding groove. The relaxation dispersion experiments detected that the free AF-6 PDZ domain was sampling multiple conformations; millisecond dynamics mapped a network for allostery signal transmission throughout the AF-6 PDZ domain in the weak saturation state, and intramolecular motions were observed in distal surface 1 when the protein was saturated. These results provide evidence that the allosteric process in the AF-6 PDZ domain is not two-state; instead, the millisecond dynamic network provides a mechanism for the transmission of allosteric signals throughout a protein. Interestingly, the two distal surfaces of the AF-6 PDZ domain respond differently to peptide binding; distal surface 1 changes in millisecond dynamics, whereas distal surface 2 undergoes structural rearrangement. The significance of the different response patterns in the signaling pathway and its relevance to the function of the AF-6 PDZ domain should be studied further.

The PDZ[1] (postsynaptic density-95, disks large, zonula occludens-1) domains are structurally conserved protein interaction modules of ∼90 residues folded into a compact globular structure of six β-strands and two α-helices (*1*). The predominant function of the PDZ domain is to recognize the extreme C-termini of other proteins, such as receptors or ion channels (*2*). Some PDZ domains also recognize internal motifs (*3*). As a protein interaction domain, the PDZ domain plays a central role in mediating both signaling protein regulation and signaling complex assembly (*2*).

The human AF-6 is a scaffold protein that links cell membrane-associated proteins and the actin cytoskeleton (*4*). It is essential for structural organization of the cell−cell junction of polarized epithelia (*5*) and plays an important role in cell−cell junctions and signal transduction (*4*). AF-6 is a large multidomain protein with a PDZ domain in the C-terminus that may function as a docking site for other molecules (*6*). It can be phosphorylated by the protein kinase Bcr (breakpoint cluster region protein), which in turn allows efficient binding of the C-terminus of Bcr to the PDZ domain of AF-6 and consequently increases the binding affinity of AF-6 for Ras. Formation of the AF-6−Bcr−Ras ternary complex results in downregulation of the Ras-mediated signal transduction pathway (*7*). In this process, AF-6 acts as a bifunctional molecule that binds Bcr via its PDZ domain and activates Ras via its Ras-binding domain (*7*). The structures of the AF-6 PDZ domain (Protein Data Bank entry 1T2M) (*6*) and the PDZ−Bcr peptide complex (Protein Data Bank entry 2AIN) (*8*) have already been determined and reveal that the C-terminal peptide of Bcr binds to the PDZ domain by fitting into a hydrophobic groove between the second β-strand (βB) and the second α-helix (αB). The pathway of the signal transfer within the AF-6 PDZ domain in the downregulation process of Ras signaling is still not clear, but allostery may play an important role in this process (*9*−*12*).

When a protein interacts with a peptide, besides the structural rearrangement, the dynamics of the protein may also play a role in the specific recognition and energetic signal transduction during the binding process (*9*, *10*, *13*, *14*). Therefore, studies of the dynamic behaviors of proteins during peptide binding are important in the development of a thorough understanding of the whole process of protein−peptide interaction. Dynamic processes in biomolecules cover a large time scale regime from picoseconds to seconds (*10*), wherein two time windows, the picosecond to nanosecond and microsecond to millisecond regimes, can be accessed by solution NMR spin relaxation experiments. NMR relax-

† This work was supported by the Chinese National Fundamental Research Project (Grants 2002CB713806, 2006CB806507, and 2006CB910201) and the Chinese National Natural Science Foundation (Grants 30121001, 30570361, and 30670426).

* To whom correspondence should be addressed: School of Life Sciences, University of Science and Technology of China, Hefei, Anhui 230026, People's Republic of China. Telephone: 86-551-3600394. Fax: 86-551-3600374. E-mail: wujihui@ustc.edu.cn.

[1] Abbreviations: AF-6, ALL-1 fusion partner from chromosome 6; PDZ, postsynaptic density-95, disks large, zonula occludens-1; Bcr, breakpoint cluster region protein; HSQC, heteronuclear single-quantum coherence; CPMG, Carr−Purcell−Meiboom−Gill.

10.1021/bi701303p CCC: $37.00
Published on Web 12/04/2007

ation experiments aiming at the picosecond to nanosecond time scale can describe the changes in protein configurational entropy during allosteric processes such as ligand binding, chemical modification, or point mutation (*15*−*17*). In these processes, dynamics changes occur at multiple amino acid sites throughout the whole protein structure, which may form the pathway optimizing energetic coupling between functionally important residues (*9*, *11*). However, these experiments cannot precisely describe the millisecond time scale motions of proteins, which are more important for allosteric processes. NMR relaxation dispersion experiments are promising methods for the exploration of biological phenomena of proteins on the millisecond time scale (*18*, *19*), such as enzyme catalysis (*20*, *21*), rate-limiting conformational exchange (*22*−*24*), disulfide bond isomerization (*25*), protein folding (*18*, *26*, *27*), interaction of protein with ligand or protein (*14*, *28*, *29*), and allostery (*13*, *30*, *31*).

To further characterize the changes in protein structure and dynamics of the AF-6 PDZ domain during peptide binding, we obtained a dissociation constant of the interaction between the AF-6 PDZ domain and Bcr peptide using NMR titration and analyzed the millisecond dynamics of free AF-6 PDZ domains, the PDZ domain with weak saturation, and the PDZ−Bcr peptide complex. The results show that the unliganded AF-6 PDZ domain is already sampling multiple conformations and the millisecond dynamics may also play a role in the energetic signal transduction of the AF-6 PDZ domain upon Bcr peptide binding. In these processes, the structural rearrangement and millisecond dynamics may play distinct roles.

MATERIALS AND METHODS

Expression and Purification of the AF-6 PDZ Domain. The gene of the human AF-6 PDZ domain (amino acid residues 987−1078) was amplified from the human brain cDNA library and inserted into the pET22b(+) plasmid (Novagen) as described previously (*6*). It was expressed as a His tag fusion protein in *Escherichia coli* BL21(DE3) by induction with 0.1 mM IPTG at 25 °C overnight. Uniformly ^{15}N-labeled proteins were prepared by growing the bacteria in SV40 medium using $^{15}NH_4Cl$ (0.5 g/L) as an exclusive isotope source. Recombinant AF-6 PDZ was purified using Hitrap chelating column (Pharmacia) chromatography. The purified protein was confirmed by SDS−PAGE, and the concentrations were determined with the BCA method.

Peptide Synthesis and Purification. The C-terminal peptide of Bcr (KRQSILFSTEV) was chemically synthesized using standard FMOC chemistry at Shanghai Zillion Pharmaceuticals Co., Ltd. The synthetic peptide was purified by a reverse-phase HPLC C_{18} column eluted with an acetonitrile gradient from 15 to 30%. The final product was verified by electrospray mass spectrometry and NMR signal assignments.

Sample Preparation. NMR samples of 1.0 mM ^{15}N-labeled AF-6 PDZ domain were buffered in 10 mM acetate, 0.5 mM EDTA, and 10% (v/v) D_2O in 450 μL (pH 5.5). A 30 mM Bcr peptide (KRQSILFSTEV) stock solution was prepared in the same buffer.

NMR Spectroscopy. Titrations of the AF-6 PDZ domain with Bcr peptide were performed by titrating a 30 mM peptide stock solution into 1 mM solutions of the ^{15}N-labeled protein. Totally, 60 μL of unlabeled Bcr peptide was added step by step during the titration until the PDZ was saturated. The ^{1}H and ^{15}N resonance variations were followed at 295 K by conducting HSQC experiments at Bruker DMX500.

Relaxation-compensated CPMG (rcCPMG), even-echo CPMG, and Hahn-echo CPMG experiments (*32*) were performed with the ^{15}N-labeled AF-6 PDZ domain samples at 295 K with two static magnetic fields, corresponding to proton Larmor frequencies of 500 and 600 MHz. The delays between the centers of two consecutive 180° pulses in the Carr−Purcell−Meiboom−Gill (CPMG) segment (τ_{CP}) were set to 1.0, 1.25, 1.5, 1.85, 2.15, 2.5, 3.0, 3.75, 4.25, 5, 6.6, 7.5, 10, 10.8, 21.5, and 64.5 ms. Spectra were acquired with at least 1024 × 128 complex points with constant relaxation delays of 0 or 60 ms. All NMR spectra were processed with NMRPipe and Sparky.

Relaxation dispersion experiments were performed for samples in three states: the free AF-6 PDZ domain sample, the AF-6 PDZ domain sample with weak saturation (molar ratio of Bcr peptide to PDZ domain of 0.1:1), and the saturated AF-6 PDZ domain (molar ratio of Bcr peptide to PDZ domain of 4:1).

Measurement of Equilibrium Dissociation Constants. Dissociation constants of the AF-6 PDZ domain for the Bcr peptide were obtained by monitoring the chemical shift changes between the AF-6 PDZ domain in the free and bound conformations during titration experiments. When the exchange rate is greater than the chemical shift difference between the free and bound states (as for the peptidic ligand in this study), the observed chemical shift at each titration point (δ_{av}) is a weighted average between the chemical shifts of the free and bound states (*33*−*35*) obtained by

$$\delta_{av} = \frac{[P_B]}{[P_T]}\delta_B + \left(1 - \frac{[P_B]}{[P_T]}\right)\delta_F \quad (1)$$

where δ_F is the chemical shift of the protein domain in the absence of peptide, δ_B is the chemical shift of the protein domain bound to peptide, $[P_B]$ is the concentration of ligand-bound protein domain, and $[P_T]$ is the total concentration of protein domain. The mole fraction used to fit the titration curve was calculated for the total substrate concentration at each point in the titration and from the fitted dissociation constant with eqs 1 and 2 using OriginPro 7.5 (OriginLab Corp.). In eq 2, K_D is the dissociation constant and $[S_T]$ is the total peptide concentration at each titration point.

$$[P_B] = \{(K_D + [S_T] + [P_T]) - [(K_D + [S_T] + [P_T])^2 - 4[S_T][P_T]]^{1/2}\}/2 \quad (2)$$

Relaxation Dispersion Analysis. Chemical exchange on a micro- to millisecond time scale increases the value of R_2 by the contribution of R_{ex}. In the measured transverse relaxation time, the exchange contribution R_{ex} is minimal during fast refocusing rates in CPMG pulse trains and increases with the τ_{cp} delays. According to eq 3 for general two-site exchange, relaxation dispersion curves depend on the chemical shift difference ($\Delta\omega$), the population of the two states (p_a and p_b), and the exchange rate (k_{ex}).

The dynamics parameters $\Delta\omega$, p_a, and k_{ex} were determined by fitting relaxation dispersion curves with the general

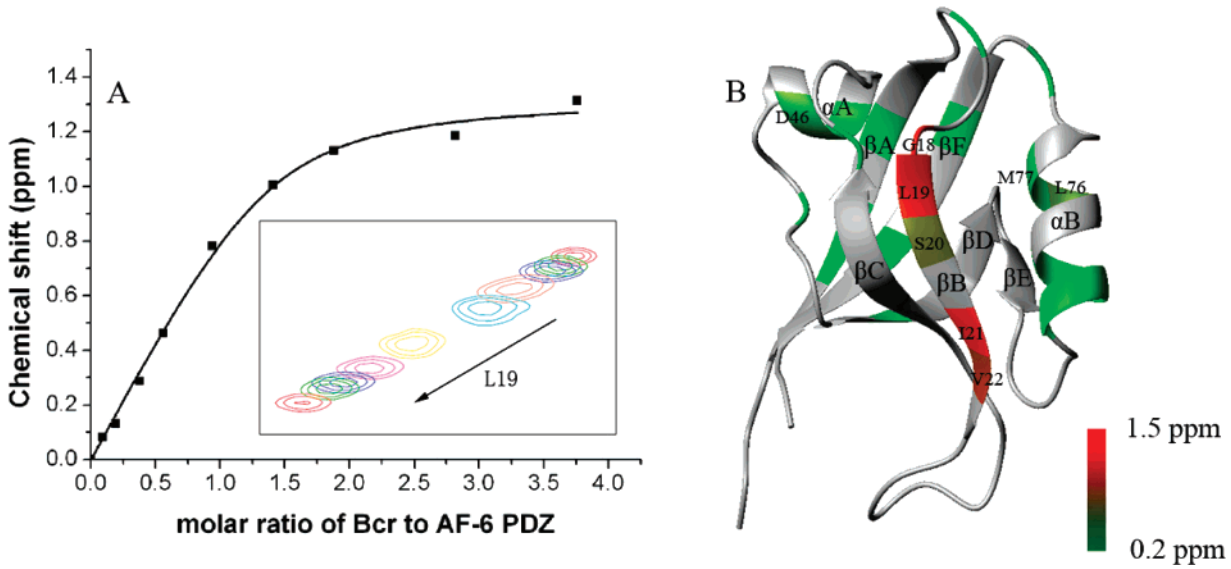

FIGURE 1: Results of chemical shift perturbation. In panel A, the inset shows the $^{1}H-^{15}N$ HSQC spectra illustrating the significant chemical shift change of Leu19 upon titration with the Bcr peptides. The contour plots, going from left to right, correspond to the values of the molar ratio of Bcr peptide to AF-6 PDZ domain, 0.1, 0.2, 0.4, 0.6, 1, 1.5, 2, 3, and 4, respectively. The black squares represent the measured changes in chemical shift for residue Leu19, and the solid line is the fitted curve. In panel B, the ^{15}N chemical shift perturbation ($\Delta\delta_N$) is color-coded on the ribbon diagram of the AF-6 PDZ domain. Residues with chemical shift differences larger than the average value ($\Delta\delta_N > 0.23$ ppm) during the peptide titration are colored with a continuous color scale from green to red that depicts $\Delta\delta_N$ values from 0.2 to 1.5 ppm, and residues with chemical shift differences smaller than the average value ($\Delta\delta_N \leq 0.23$ ppm) are colored gray. Residues with significant chemical shift changes ($\Delta\delta_N \geq 0.5$ ppm) during the peptide titration are labeled.

expression of transverse relaxation rate R_2 in two-site exchange in which $p_b = 1 - p_a$ (*36*−*38*)

$$R_2(1/\tau_{CP}) = \frac{1}{2}\left\{R_a + R_b + k_{ex} - \frac{1}{\tau_{CP}}\cosh^{-1}[D_+\cosh(\eta_+) - D_-\cos(\eta_-)]\right\}$$

$$D_\pm = \frac{1}{2}\left[\pm 1 + \frac{\psi + 2\Delta\omega^2}{(\psi^2 + \zeta^2)^{1/2}}\right]$$

$$\eta_\pm = \frac{\tau_{CP}}{\sqrt{2}}[\pm\psi + (\psi^2 + \zeta^2)^{1/2}]^{1/2}$$

$$\psi = (R_a - R_b - p_a k_{ex} + p_b k_{ex})^2 - \Delta\omega^2 + 4p_a p_b {k_{ex}}^2$$

$$\zeta = 2\Delta\omega(R_a - R_b - p_a k_{ex} + p_b k_{ex}) \quad (3)$$

Only minor differences were observed in the dispersion curves obtained by simulation of eq 3 with different relaxation rates R_a and R_b and by simulation with $R_a = R_b = R_2^0$ for the amide nitrogens of sites a and b (*29*). Therefore, we assumed that R_a and R_b are equal and fit the experimental $R_2(\tau_{cp}^{-1})$ values as a function of $1/\tau_{cp}$ with eq 3 using OriginPro 7.5. The Levenberg−Marquardt algorithm was used in the curve fitting.

RESULTS

Interaction of the AF-6 PDZ Domain with Bcr Peptide Yields Conformation Changes beyond the Peptide Binding Groove. The solution structures of the AF-6 PDZ domain and AF-6 PDZ−Bcr peptide complex have been determined, and the chemical shift behavior of AF-6 PDZ during Bcr peptide binding has been analyzed (*6*, *8*). Comparison of the AF-6 PDZ domain structure in free and complex forms shows that residues from helix αA exhibit an obvious deviation with a rmsd value of 1.13 Å beyond the peptide binding groove, which is consistent with the result of chemical shift perturbation (*8*).

Table 1: Dissociation Constants for the Interaction of the AF-6 PDZ Domain with Bcr Peptide

residue[a]	K_D (mM)	standard error[b]
G18	0.12	0.03
L19	0.12	0.04
S20	0.22	0.08
V22	0.13	0.04
A23	0.14	0.04
A45	0.11	0.04
D46	0.09	0.05
S81	0.24	0.07

[a] Most residues are those located at the βB and αA region, the chemical shift changes of which are significant during titration with the C-terminal peptide of Bcr. [b] Dissociation constants (K_D) were determined from NMR titrations as described in Materials and Methods.

To further analyze the interaction between the AF-6 PDZ domain and Bcr peptide, we repeated titration experiments of the Bcr peptide with the AF-6 PDZ domain to obtain the dissociation constant of the interaction and mapped the residues experiencing ^{15}N chemical shift changes onto the structure of the AF-6 PDZ domain (Figure 1). As mentioned previously (*6*), eight residues exhibited significant shift changes during the titration and dissociation constants were calculated from those chemical shift changes (Table 1). The result shows that most residues have similar dissociation constants of ~0.12 mM, except residues S20 (0.22 mM) and S81 (0.24 mM). Interestingly, though ~12 Å from the center of the peptide binding site in βB, residues A45 and D46 in αA have similar dissociation constants (0.11 and 0.09 mM, respectively) with residues G18 (0.12 mM), L19 (0.12 mM),

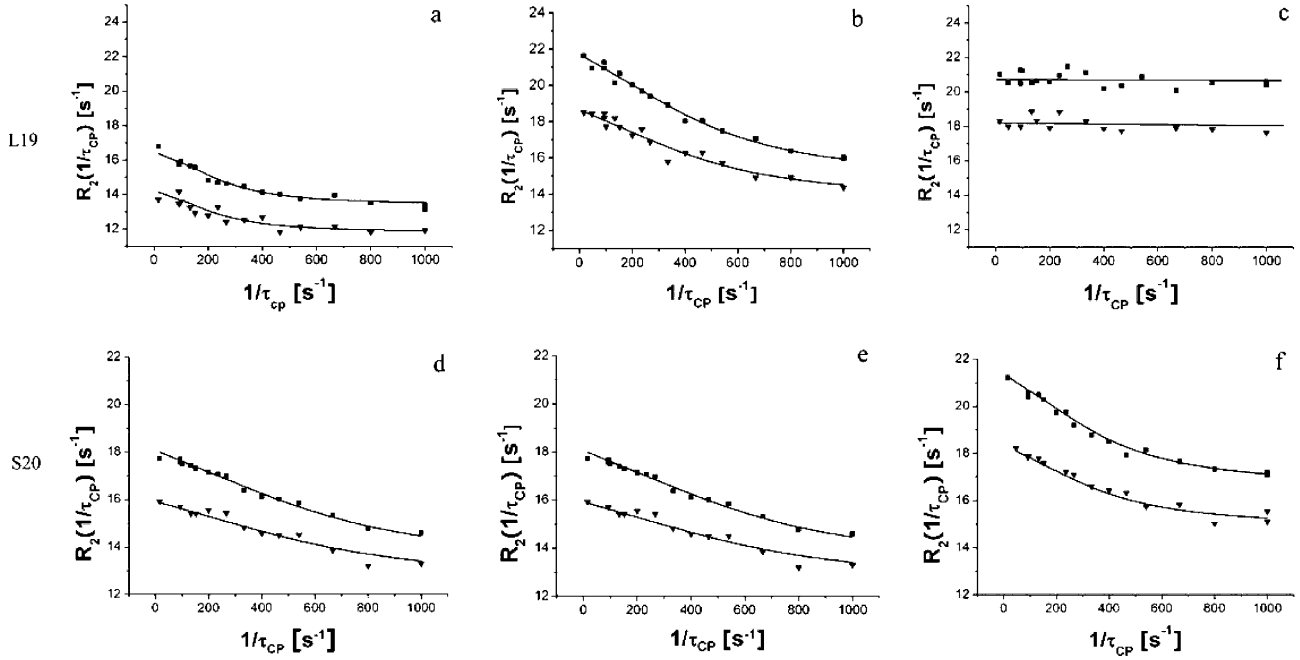

FIGURE 2: Relaxation dispersion curves for residues L19 (a) and S20 (d) in free PDZ, L19 (b) and S20 (e) in the weak saturation state, and L19 (c) and S20 (f) in the PDZ−Bcr complex. Data were recorded at ^{1}H Larmor frequencies of 500 (▼) and 600 MHz (■).

and V22 (0.13 mM) that are located at the binding groove, indicating that all these residues may report on the same binding event (*13*).

The dissociation constants measured by NMR titration are ~50 times higher than that previously measured by BIAcore (*6*). However, the NMR chemical shift data give a much more sensible result with affinities in the millimolar range (*35*) which would be difficult to be probed by BIAcore analysis. Furthermore, the isothermal titration calorimetry (ITC) (*39*) experiment was performed to verify the dissociation constant of the AF-6 PDZ domain for Bcr peptide measured by NMR titration. The dissociation constant measured by isothermal titration calorimetry is 0.25 mM (Figure S1 of the Supporting Information). Thus, the dissociation constants of 0.1−0.2 mM may be more reliable for the interaction between the AF-6 PDZ domain and Bcr peptide. The dissociation constant (K_D) is important for the quantitative description of the exchange process in the following text. So we calculated the population (p_a) and the exchange rate (k_{ex}) using K_D values of 0.12 and 0.25 mM, respectively. Only minor differences were observed when we calculated the parameters using those two different K_D values. Therefore, we assumed $K_D = 0.12$ mM to calculate the population (p_a) and the exchange rate (k_{ex}) in the following text.

Conformational Exchange in Free PDZ. To further analyze the process of peptide binding on the millisecond time scale, we performed ^{15}N transverse relaxation dispersion experiments on the free AF-6 PDZ domain, the AF-6 PDZ domain with weak saturation, and an AF-6 PDZ domain−Bcr peptide complex. For the free AF-6 PDZ domain, relaxation dispersion curves were analyzed for 88 residues, the resonances of which were not overlapped in the ^{15}N HSQC spectrum. Examples of typical dispersion curves of residues L19 and S20 are shown in panels a and d of Figure 2. The transverse relaxation rate R_2 of most residues was not influenced by the variation of τ_{cp} in the CPMG sequence, which meant no contribution of R_{ex} to the transverse relaxation rate R_2 of these residues. Sixteen residues were observed with R_{ex} resulting from exchange contributions. These residues are listed in Table 2 and depicted in Figure 3A on a ribbon diagram of the free AF-6 PDZ domain in colors from green (0.5 s^{-1}) to red (13 s^{-1}) for increasing values of R_{ex}.

R_{ex}, the exchange contribution to the transverse relaxation rate R_2, is considered a qualitative measurement of the exchange process on the microsecond to millisecond time scale. The values of R_{ex} are mostly ~1−3 s^{-1} in the free PDZ domain except for residue G18 ($R_{ex} = 7.3$ s^{-1}), and the average exchange contribution R_{ex} is ~2.3 s^{-1} (Table 2 and Figure 3A). As shown in Figure 3A, there was a good correlation between residues undergoing conformational exchange and those involved in peptide binding. Eleven of the 16 residues which exhibited conformational exchange were located in the peptide binding groove, the αB−βB groove, and the βB−βC loop. Exchange contributions were also observed in the βF strand, the αA−βD loop, and the C-terminus of the βE−αB loop.

Exchange rates are also mapped in Figure 4A on the ribbon diagram of the free AF-6 PDZ domain using a color scale from green (100 s^{-1}) to red (3000 s^{-1}). As shown in Table 2, the exchange rates are no more than 1000 s^{-1} for most parts of the free AF-6 PDZ domain. The residues in the βB strand exhibit exchange rates of ~500−1000 s^{-1}. Considering the uncertainty, these residues may be considered to exchange between sites with similar k_{ex} values. Lower exchange rates are observed for the residues in the αB helix. For example, exchange rates of residues E71, A73, and A74 are ~200−300 s^{-1}.

In a previous study, the concentration-dependent chemical shift change is investigated over a concentration range from 0.275 to 2 mM (*8*). Only a few cross-peaks exhibited small chemical shift perturbations, less than 0.04 ppm in the ^{1}H and 0.4 ppm in the ^{15}N dimension. Furthermore, a standard backbone (^{15}N) T_2 relaxation experiment (*40*) has been used

Table 2: ^{15}N Relaxation Dispersion Parameters of Exchanging Residues of Free PDZ

residue	R_{ex}[a] (s^{-1})	R_2^0 (s^{-1})	p_a	$\Delta\omega_{fit}$[b] (ppm)	$\Delta\omega_{titr}$[b] (ppm)	k_{ex} (s^{-1})	α[c]
G18	7.3	13.6 ± 0.5	0.980 ± 0.02	2.10 ± 0.31	1.38	1253 ± 149	1.5
L19	3.1	11.8 ± 0.1	0.987 ± 0.009	1.29 ± 0.09	1.31	620 ± 103	1.3
S20	1.8	12.4 ± 0.1	0.995 ± 0.004	2.01 ± 0.17	0.84	541 ± 189	0.7
I21	2.7	12.9 ± 0.4	0.994 ± 0.005	2.37 ± 0.29	0.06	1071 ± 253	1.3
V22	3.0	13.9 ± 0.2	0.989 ± 0.001	1.52 ± 0.16	1.54	818 ± 163	1.4
Q29	1.9	9.4 ± 0.08	0.99 ± 0.01	1.11 ± 0.11	0.01	698 ± 128	1.5
K31	0.8	9.0 ± 0.03	0.996 ± 0.001	0.99 ± 0.10	0.05	348 ± 82	1.0
L32	1.6	11.1 ± 0.1	0.990 ± 0.003	0.91 ± 0.25	0.22	237 ± 40	0.7
I34	2.1	13.7 ± 0.2	0.99 ± 0.01	1.09 ± 0.14	0.11	501 ± 161	1.3
R50	3.0	14.1 ± 0.7	0.995 ± 0.005	3.2 ± 0.76	0.13	1612 ± 239	1.4
L68	1.4	11.3 ± 0.08	0.990 ± 0.005	1.03 ± 0.17	0.02	168 ± 38	0.4
S69	1.4	11.9 ± 0.1	0.995 ± 0.002	1.51 ± 0.14	0.17	574 ± 146	1.1
E71	2.4	11.9 ± 0.1	0.987 ± 0.002	0.98 ± 0.06	0.35	289 ± 85	0.8
A73	1.2	11.9 ± 0.1	0.995 ± 0.002	1.82 ± 0.35	0.37	280 ± 58	0.3
A74	1.4	11.9 ± 0.06	0.990 ± 0.002	0.83 ± 0.14	0.19	199 ± 55	0.6
E87	1.4	12.8 ± 0.1	0.992 ± 0.009	0.90 ± 0.11	0.24	408 ± 144	1.3

[a] $R_{ex} = R_2(1/\tau_{CP}\rightarrow 0) - R_2(1/\tau_{CP}\rightarrow\infty)$ at a static magnetic field of 14.1 T. [b] $\Delta\omega_{fit}$, chemical shift difference obtained from dispersion profiles using eq 3, not given when $\Delta\omega_{titr}$ was used to fit the data; $\Delta\omega_{titr}$, chemical shift difference of the amide nitrogen between free PDZ and the PDZ−Bcr complex. [c] $\alpha = [(B_{02} + B_{01})/(B_{02} - B_{01})]/[(R_{ex2} - R_{ex1})/(R_{ex2} + R_{ex1})]$, where R_{ex1} and R_{ex2} are the values of R_{ex} measured at B_{01} (11.7 T) and B_{02} (14.1 T), respectively (*32*).

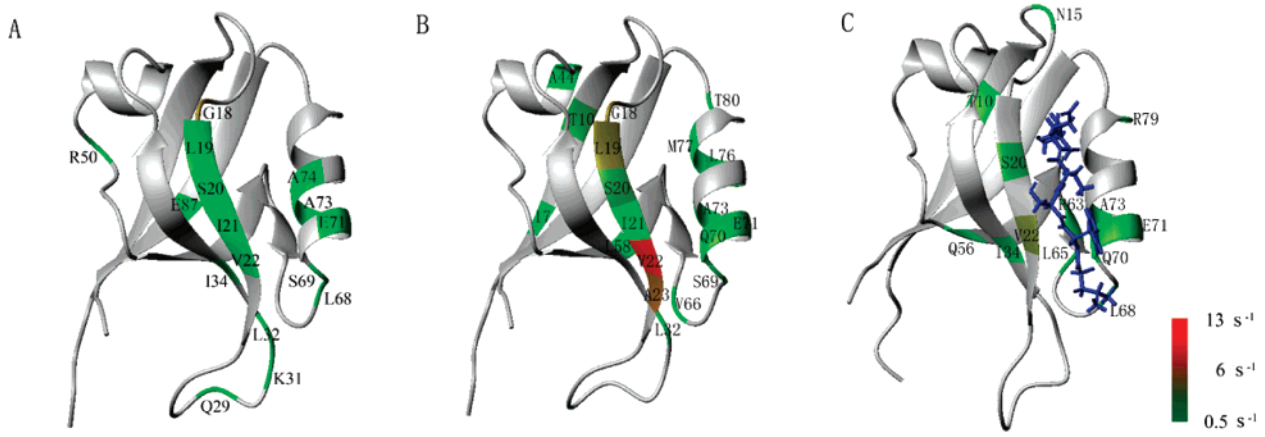

FIGURE 3: Exchange contributions for the free AF-6 PDZ domain (A), PDZ in the weak saturation state (B), and the PDZ−Bcr complex (C). The exchange contribution R_{ex} is color-coded on the ribbon diagram of PDZ. A continuous color scale from green to red (from 0.5 to 13 s^{-1}) depicts R_{ex} values. Residues colored gray do not exhibit conformation exchange or cannot be analyzed due to overlapping or missing assignments.

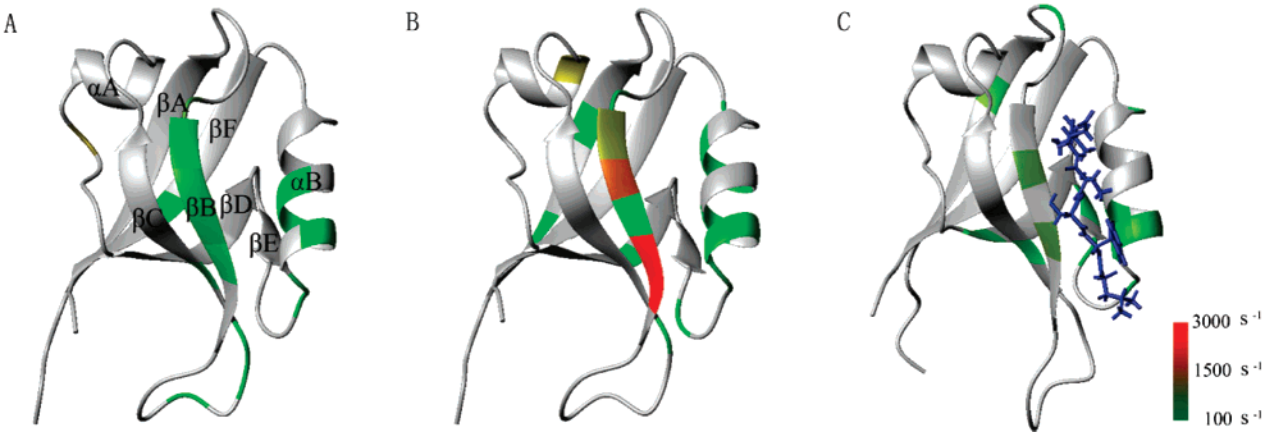

FIGURE 4: Exchange rates in the free AF-6 PDZ domain (A), PDZ in the weak saturation state of PDZ (B), and the PDZ−Bcr complex (C). The k_{ex} exchange rates are color-coded on the ribbon diagram of PDZ. A continuous color scale from green to red (from 100 to 3000 s^{-1}) depicts k_{ex} values. Residues colored gray do not exhibit conformation exchange or cannot be analyzed due to overlapping or missing assignments.

to collect R_2 data at 500 MHz at protein concentrations of 0.5 and 1 mM, respectively. The results verified that the dynamics parameters were not concentration-dependent from 0.5 to 1 mM (Figure S2 of the Supporting Information). Therefore, the degree of the possible dimerization of the AF-6 PDZ domain should be too low to affect the observed

Table 3: ^{15}N Relaxation Dispersion Parameters of Exchanging Residues of PDZ in the Weak Saturation State (molar ratio of Bcr peptide to PDZ domain of 1:10)

residue	R_{ex} (s^{-1})	R_2^0 (s^{-1})	p_a	$\Delta\omega_{titr}$ (ppm)	$\Delta\omega_{fit}$ (ppm)	k_{ex} (s^{-1})	α
I7	2.9	14.9 ± 0.1	0.92 ± 0.01	0.36	−	464 ± 87	1.9
T10	5.1	19.8 ± 0.4	0.97 ± 0.03	0.41	2.14 ± 0.31	179 ± 17	0.1
G18	7.2	15.7 ± 0.2	0.972 ± 0.006	1.38	−	678 ± 135	1.4
L19	6.9	13.7 ± 0.4	0.953 ± 0.006	1.31	−	1503 ± 114	1.8
S20	5.1	12.5 ± 0.1	0.88 ± 0.03	0.84	−	2120 ± 202	0.7
I21	1.5	13.2 ± 0.07	0.995 ± 0.004	0.06	1.85 ± 0.16	470 ± 126	0.7
V22	11.1	14.8 ± 0.5	0.89 ± 0.005	1.54	−	≈3000	1.9
A23	>6	−	−	1.12	−	3000−5000	−
L32	2.9	10.9 ± 0.1	0.98 ± 0.04	0.22	0.96 ± 0.09	752 ± 134	1.7
A44	1.8	12.7 ± 0.3	0.996 ± 0.007	*a*	2.57 ± 0.47	1578 ± 182	1.5
L58	2.0	13.9 ± 0.1	0.990 ± 0.006	0.08	1.11 ± 0.17	289 ± 156	0.7
V66	1.6	11.6 ± 0.1	0.98 ± 0.09	0.15	0.52 ± 0.07	382 ± 84	1.6
S69	1.7	12.0 ± 0.1	0.995 ± 0.003	0.17	1.76 ± 0.15	808 ± 102	1.3
Q70	3.6	13.2 ± 0.04	0.81 ± 0.01	0.31	−	580 ± 52	1.9
E71	3.4	12.9 ± 0.06	0.83 ± 0.02	0.35	−	468 ± 92	1.9
A73	1.9	12.1 ± 0.05	0.937 ± 0.009	0.37	−	597 ± 134	1.9
L76	3.6	12.7 ± 0.06	0.967 ± 0.003	0.73	−	571 ± 69	1.7
M77	1.8	13.2 ± 0.06	0.974 ± 0.003	0.55	−	532 ± 84	1.8
T80	3.3	9.3 ± 0.1	0.98 ± 0.01	0.04	0.86 ± 0.07	379 ± 92	1.2

[a] The residue disappeared in complex PDZ.

relaxation dispersion curves, and the millisecond dynamics of the free AF-6 PDZ domain should not be influenced by the possible dimerization.

A Low Concentration of Bcr Peptide Induces Significant Dynamical Changes. Due to the weak binding between the Bcr peptide and PDZ domain (K_D = 0.12 mM), the conformational exchange between free PDZ and the complex form can contribute significantly to the measured R_{ex} values. When we studied the millisecond dynamics of the AF-6 PDZ domain during peptide binding, we were forced to separate chemical exchange induced by the intrinsic dynamics from chemical exchange between free PDZ and the complex form. To solve this problem, we added small amount of Bcr peptide to the PDZ domain (molar ratio of Bcr peptide to PDZ domain of 1:10) and analyzed the millisecond dynamics in the weak saturation state.

Slight resonance shifts were observed in ^{15}N HSQC after a small amount of peptide addition, whereas the millisecond dynamics changed significantly. In the weak saturation state, 19 residues exhibited conformational exchange, and the average exchange contribution (R_{ex}) was 3.9 s^{-1}, much larger than that in the free PDZ state (2.3 s^{-1}) (Table 3 and Figure 3B), indicating an increase in the number of conformational exchanges of the PDZ domain. This sudden increase in the conformational exchange contribution to transverse relaxation after addition of a small amount of peptide was consistent with the previous study of protein−ligand interaction (*29*), which suggested the rearrangement was induced by Bcr peptide binding and direct protein−peptide interaction. Most of the residues undergoing conformational exchange were located around the αB−βB groove where the Bcr peptide bound. Interestingly, some residues distal from the peptide binding groove also underwent significant changes in exchange contributions compared with that in the free state; for example, residues I7, T10, A44, and L58 started chemical exchange, whereas residues I34, R50, and E87 exhibited no chemical exchange.

When the chemical shifts of the two exchanging states are known, $\Delta\omega$ can be fixed at the value of the chemical shift difference of those two states upon the relaxation dispersion data fitting. If exchange in the weak saturation state is induced by the addition of Bcr peptide for the AF-6 PDZ domain, the two exchanging partners are most likely the free and complex states of the protein. Therefore, upon relaxation dispersion data fitting of the weak saturation state and the complex state, we first set $\Delta\omega$ to the values of the ^{15}N chemical shift difference between the free and complex in the ^{15}N HSQC spectrum ($\Delta\omega_{titr}$), and then some residues which could not be fitted with $\Delta\omega_{titr}$ stood out, indicating that there were other millisecond dynamics besides the conformational exchange between free and complex forms (*29*).

In the relaxation dispersion data fitting, 10 of the 19 residues which exhibited conformational exchange in the weak saturation state could be successfully fitted with the chemical shift differences between the free and complex states ($\Delta\omega_{titr}$), which indicated that the conformational exchange occurred between free and complex forms. For those residues, the populations of the predominant state obtained by fitting eq 3 to the relaxation dispersion data were between 0.81 and 0.97 (Table 3), which were concordant with the population (92%) calculated from the measured K_D value [0.12 mM (Table 1)]. Most of those residues (I7, G18, Q70, E71, A73, L76, and M77) had similar exchange rates of ∼500∼600 s^{-1}.

We analyzed the line shapes of residue G18 (Figure S3A of the Supporting Information). Line shapes of residue G18 show a general two-step exchange process between free and complex forms

$$P + L \underset{k_{on}}{\overset{k_{off}}{\rightleftharpoons}} PL \qquad (4)$$

The exchange rate k_{ex} equals $k_{on}[L] + k_{off}$, where [L] is the concentration of the free ligand (*19*, *29*). Thus, the simulated off rate (k_{off} = 550 s^{-1}) can be used to determine the rate of exchange between free and complex forms in that state. For the interaction of the AF-6 PDZ domain and Bcr peptide, the measured dissociation constant K_D ($=k_{off}/k_{on}$) is ∼0.12 mM. When the total protein concentration is 1 mM and the total concentration of Bcr peptide is 0.1 mM, the concentra-

Table 4: ^{15}N Relaxation Dispersion Parameters of Exchanging Residues of the PDZ−Bcr Complex

residue	R_{ex} (s^{-1})	R_2^0 (s^{-1})	p_a	$\Delta\omega_{titr}$ (ppm)	$\Delta\omega_{fit}$ (ppm)	k_{ex} (s^{-1})	α
T10	2.8	17.1 ± 0.5	0.83 ± 0.09	0.41	−	1041 ± 239	1.9
N15	2.4	13.0 ± 0.2	0.99 ± 0.01	0.29	1.08 ± 0.11	543 ± 99	1.4
S20	4.9	14.9 ± 0.2	0.931 ± 0.007	0.84	−	1290 ± 98	1.9
V22	6.5	20.5 ± 0.8	0.989 ± 0.002	1.54	−	1337 ± 269	1.7
I34	1.9	14.3 ± 0.1	0.98 ± 0.01	0.11	0.83 ± 0.57	142 ± 20	0.4
Q56	1.3	14.5 ± 0.1	0.93 ± 0.02	0.34	−	865 ± 268	1.9
R63	1.0	10.7 ± 0.1	0.99 ± 0.04	0.11	1.41 ± 0.31	105 ± 15	0.1
L65	1.7	14.7 ± 0.1	0.994 ± 0.002	0.002	1.73 ± 0.42	356 ± 107	0.5
L68	1.3	11.9 ± 0.1	0.993 ± 0.002	0.02	1.07 ± 0.26	277 ± 134	0.7
Q70	2.6	14.5 ± 0.1	0.990 ± 0.002	0.31	1.95 ± 0.16	305 ± 25	0.3
E71	3.7	14.2 ± 0.1	0.98 ± 0.02	0.35	1.25 ± 0.07	850 ± 81	1.6
A73	1.2	13.3 ± 0.1	0.994 ± 0.003	0.37	1.18 ± 0.40	251 ± 127	0.5
R79	1.6	11.4 ± 0.1	0.995 ± 0.002	0.09	1.70 ± 0.16	678 ± 140	1.1

tion of bound protein is ∼0.08 mM according to eq 2 and the concentration of free peptide is ∼0.02 mM. Therefore, the calculated rate of exchange between free and complex forms in this state is ∼640 s^{-1} ($k_{ex} = k_{on}[L] + k_{off} = 550/0.12\ mM^{-1}\ s^{-1} \times 0.02\ mM + 550\ s^{-1} \approx 640\ s^{-1}$), which approaches the exchange rates measured in relaxation dispersion experiments (∼500−600 s^{-1}) in the weak saturation state.

For exchange between free and complex forms, the measured exchange rates in the weak saturation state should be relatively homogeneous. However, some residues in the βB strand had much higher exchange rates of ∼1500−3000 s^{-1}, such as L19 ($k_{ex} = 1503 \pm 114\ s^{-1}$), S20 ($k_{ex} = 2120 \pm 202\ s^{-1}$), and V22 ($k_{ex} \approx 3000\ s^{-1}$). In addition, residue A23 exhibited an exchange rate of 3000−5000 s^{-1}, which could not be properly fitted with eq 3. Residue I21 in the βB strand exhibited a slight chemical shift difference in the ^{15}N dimension during peptide titration and a relatively low exchange rate of ∼500 s^{-1}, which could be due to the fact that the side chain of I21 might have a different orientation compared to that of adjacent residues and it might not interact with the Bcr peptide directly (*8*) (Table 3 and Figure 3B). The relatively high exchange rates of the residues in the βB strand may be a consequence of the systematic error made by the assumption of two-state exchange used in the analysis. If there is a set of parallel processes involved, the exchange rates measured by the CPMG method will always be higher than the real values (*29*, *41*).

This assumption agrees with the line shapes of residue A23, too. The line shapes of A23 are more complex than those of G18, and the two minor shoulders of the labeled peak indicate multiple states at some points during the titration (Figure S3B of the Supporting Information) (*41*, *42*). The results of line shape analysis of residues G18 and A23 are consistent with that of dispersion analysis and support the assumption that in the weak saturation state, the AF-6 PDZ domain exchanges between free and complex forms and some intermediates are involved in that process.

In the dispersion data fitting of the weak saturation state, the last eight of the 19 residues which exhibited conformational exchange in this state could not be fitted with the chemical shift differences between the free and complex states (Table 3), and these residues exhibited relatively small chemical shift differences during the peptide titration. Thus, the chemical exchange of these residues could not be attributed to the conformational exchange between free and complex forms. Moreover, populations fitted from the dispersion data of those residues were mostly ∼98−99%. Chemical exchanges of those residues could be contributed by the intrinsic dynamics of the protein.

Thus, in the weak saturation state, the total 19 residues undergoing conformational exchange can be partitioned into three kinds of dynamic processes: residues I7, G18, Q70, E71, A73, L76, and M77 seem simply to exchange between free and complex forms, residues T10, I21, L32, A44, L58, V66, S69, and T80 seem to undergo intrinsic conformational exchange, and residues L19, S20, V22, and A23 may undergo conformational exchange between free and complex forms with some other intermediates involved in their exchange processes. In another view, some small events on the millisecond time scale may be introduced by the low-concentration peptide besides the conformational exchange between free and complex forms.

The AF-6 PDZ Domain Saturated with Bcr Peptide Exhibits Millisecond Motions Distal from the Binding Groove. The Bcr peptide solution was added to the ^{15}N-labeled AF-6 PDZ domain until the AF-6 PDZ domain was saturated (molar ratio of Bcr peptide to PDZ domain of 4:1) (Figure 1A). Eighty-six residues for which the resonances were not overlapped in the HSQC spectrum were analyzed. These residues included those for which no ^{15}N chemical shift perturbation was observed during the titration of Bcr peptides.

The AF-6 PDZ domain in the complex state seems to be rigid in the binding groove on the millisecond time scale. Thirteen residues undergo conformational exchange, and the average exchange contribution is 2.5 s^{-1}. The exchange rates are generally low compared with that in the weak saturation state and are in a range similar to the range of those in the free state. In the binding groove, only five residues exhibit chemical exchange (S20 and V22 in the βB strand and Q70, E71, and A73 in the αB helix), and no exchange process is observed in the βB−βC loop.

Only four residues could be fitted with $\Delta\omega_{titr}$, and the exchange rates of these residues were ∼900−1300 s^{-1} (Table 4). For two-site exchange between free and complex forms, the dynamic equilibrium can be described as eq 4, and the exchange rate k_{ex} equals $k_{on}[L] + k_{off}$. Therefore, the measured exchange rate (k_{ex}) will increase with the addition of the ligand. Considering that the rate of the conformational exchange between free and complex forms is ∼500−600 s^{-1} in the weak saturation state, those higher exchange rates (∼900−1300 s^{-1}) may reflect the rate of the exchange between free and complex PDZ in the complex state.

Some residues with relatively small chemical shift changes during peptide titration exhibit chemical exchange in the complex state. For example, residues (R63, L65, and L68) around the βE strand exhibit conformational exchange in the complex state, although peptide binding causes slight ^{15}N chemical shift changes [<0.05 ppm (Figure 1B)]. Residues L65, L68, and A73 form a hydrophobic pocket and have exchange rates of 100−300 s^{-1}, similar to that of R63. A higher exchange rate is exhibited by residue N15 (k_{ex} = 543 ± 99 s^{-1}) in the βA−βB loop.

DISCUSSION

Allostery, ligand binding in one site of a molecule that causes an effect at another site, is crucial in living cells (*43*). The allosteric process is a fundamental process by which proteins propagate signals from one site to affect functionally important sites located distally (*9*, *10*). The "concerted" or "MWC" model was proposed by Monod et al. (*44*, *45*) on the basis of the discovery of allosteric enzyme systems in 1965. Since then, people have endeavored to understand the allosteric mechanism by which signals are transmitted across long distances in proteins (*46*). Traditionally, allosteric processes are investigated by comparing the static structures of allosteric molecules in their limited states (*10*). It is often stated that allosteric systems are multidomain proteins or oligomers, such as hemoglobin (*47*) and aspirate transcarbamylase (*48*). However, recently, it was found that allosteric coupling could be introduced into monomeric proteins that were presumably nonallosteric proteins by interaction with a stronger ligand, chemical modification, or point mutation (*49*). Modern concepts of protein-folding funnels and energy landscapes treat a protein as a dynamic ensemble of conformational states. Ligand binding merely shifts the population of those conformational states. Redistribution of the molecular ensemble leads to altered conformations at some other locations (*43*). According to these classical views, allosteric processes are accompanied by a series of discrete conformational changes that alter the protein mean structure. In another view, allosteric processes could be considered to proceed solely through changes in protein dynamics without conformational changes (*50*). Recently, the work of Popovych and co-workers provided experimental support for that theory and proved the existence of purely dynamically driven allostery (*31*). To explore the role of dynamics in allosteric regulation, a number of methods are used for the detailed characterization of molecular motions and changes that occur upon interaction. Optical spectroscopy, molecular simulation, crystallography, and NMR spectroscopy are major methods used for that goal (*51*). Within them, NMR spectroscopy is unique in yielding site-specific information about multiple time scales (*10*).

The allosteric processes in PDZ domains have been studied from the perspective of structure and dynamics. Binding of Cdc42 to the cell polarity protein Par-6 induces an allosteric transition in the CRIB-PDZ module of Par-6 and increases the affinity of the Par-6 PDZ domain for its carboxy-terminal ligand by ~13-fold (*12*), and according to the main chain and side chain methyl dynamics of the second PDZ domain from human tyrosine phosphatase 1E (hPTP1E), the PDZ domain shows long-range dynamic effects that correspond to previously observed pairwise energetic couplings (*52*) upon a target peptide binding (*9*) or point mutation (*11*).

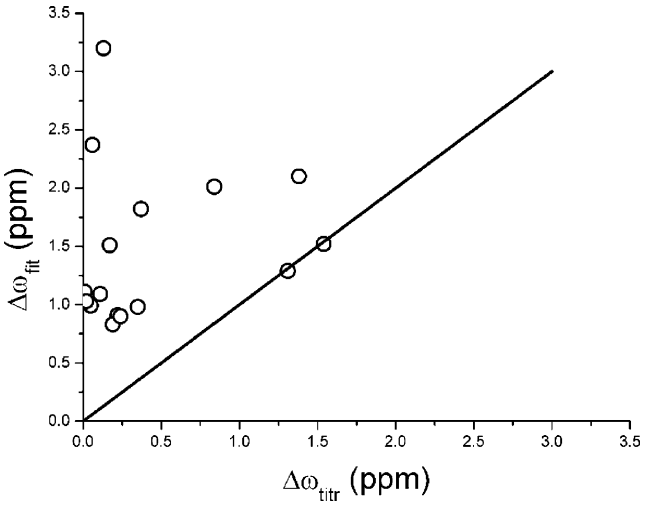

FIGURE 5: Correlations between $\Delta\omega_{fit}$ (abscissa), obtained from dispersion profiles in the free state to eq 3, and the chemical difference, $\Delta\omega_{titr}$ (ordinate), between the free and complex state of the AF-6 PDZ domain. The black line represents the correlation $\Delta\omega_{fit} = \Delta\omega_{titr}$.

Dynamic processes in proteins cover a large time scale regime from picoseconds to seconds (*10*). Fuentes and his co-workers have used NMR relaxation experiments to describe a picosecond to nanosecond dynamic network of the hPTP1E PDZ2 domain (*9*). Here we use NMR relaxation dispersion experiments to explore the dynamic network on a millisecond time scale that is more important for the allosteric process.

The Free AF-6 PDZ Domain Is Already Sampling Multiple Conformations. The solution structure of the AF-6 PDZ−Bcr peptide complex and the perturbation of NMR spectra upon Bcr peptide titration have identified the residues involved in Bcr peptide binding (*6*, *8*). Figure 1B shows the residues having significant chemical shift changes due to peptide binding. Figure 3A shows the mapping of residues undergoing conformational exchange in the free state. Clearly, there is a good correlation between residues undergoing conformational exchange and those involved in peptide binding. As shown in Table 2 and Figure 5, the chemical shift differences derived from dispersion data fitting and Bcr peptide titration are similar for only two residues, L19 and V22. Most residues have relatively large differences between those two kinds of chemical shift differences. Therefore, it seems that instead of equilibrating between free and complex conformations, the AF-6 PDZ domain samples multiple conformations in the free state.

Conformational exchange has been suggested to be a common feature of protein functions and protein−protein interactions (*10*, *53*). Flexible residues of free protein may span a larger conformational space to allow them to bind to target molecules more easily (*28*, *54*, *55*). The close correlation between AF-6 PDZ domain residues exhibiting conformational exchange and those involved in Bcr peptide binding suggests that the unliganded AF-6 PDZ domain is already sampling multiple conformations and those conformational exchanges may be essential for the interaction between the PDZ domain and Bcr peptide.

Millisecond Dynamics in the Weak Saturation State Map a Network in the AF-6 PDZ Domain. When a small amount of Bcr peptide was added to the PDZ domain solution (molar

ratio of Bcr peptide to PDZ domain of 1:10), significant changes in the millisecond dynamics of the AF-6 PDZ domain were observed (Tables 2 and 3). According to the measured K_D value [0.12 mM (Table 1)], only ~8% of the PDZ domain is complexed to the Bcr peptide in the weak saturation state. Considering the generally low exchange contributions ($R_{ex} < 5\ s^{-1}$) for nearly all the residues in the complex state, the intramolecular dynamics (these dynamics are the result of intramolecular motions instead of the interaction with peptide) of the PDZ complex are negligible in the weak saturation state.

As we have mentioned before, in the weak saturation state, many residues exchange between free and complex forms upon addition of a small amount of Bcr peptide. Some residues (I7, G18, Q70, E71, A73, L76, and M77) seem simply to exchange between free and complex forms, and although some residues (L19, S20, and V22) seem to have other millisecond motions in their exchange processes, it is difficult to distinguish intramolecular dynamics from intermolecular exchange for these residues. The main subject that we will discuss is the intrinsic dynamics of PDZ in the weak saturation state; thus, all those residues are excluded from the following discussion.

It is very interesting that millisecond dynamics change significantly after a small amount of peptide is added. When the chemical exchange contributions (R_{ex}) of the free PDZ are compared with that of the PDZ domain in the weak saturation state (Tables 2 and 3), 13 residues exhibit significant changes in millisecond dynamics. The difference in the chemical exchange contribution after and before the addition of a small amount of peptide, ΔR_{ex}, is more than 1 s^{-1}. Most of those residues are distal from the peptide binding groove (Figure 6B). The dynamical behaviors of those residues are introduced by the low concentration of peptide, and therefore, it is intriguing that the binding of Bcr peptide affects the residues distal from peptide binding groove.

Why does the binding of Bcr peptide affect the residues unassociated with the peptide binding? Is there a network in the AF-6 PDZ domain to physically link distant sites in the protein? Previously, Lockless and co-workers (*52*) identified residue−residue "thermodynamic couplings" in the PDZ family using to evolutionary data. In 2004, Fuentes and co-workers (*9*) detected the side chain dynamic response of the hPTP1E PDZ2 domain to ligand binding and identified residues "dynamically coupled" in the PDZ2 domain. Furthermore, the dynamical couplings within the hPTP1E PDZ2 domain were confirmed by the side chain ^2H dynamics of the hPTP1E PDZ2 mutants (*11*). In Figure 6A, those thermodynamically coupled residues are colored red in the amino acid sequence of PSD-95 PDZ3, and those dynamically coupled residues are colored green in the amino acid sequence of hPTP1E PDZ2.

As mentioned above, 13 residues (Figure 6A, colored blue) underwent significant changes in millisecond dynamics after a small amount of peptide was added. On the basis of the amino acid sequence alignment of AF-6 PDZ, hPTP1E PDZ2, and PSD-95 PDZ3 (Figure 6A), we can correlate those residues with the residue−residue couplings identified previously in the amino acid sequence (*9*, *52*). Six of the 13 residues are identical to the residues identified previously, such as A44, Q29, and T80, and six residues neighbor the residues identified previously (with no more than two residues in them), such as R50, E87, and L58. In total, 12 residues, or more than 90%, have correlations with the residues that were thermodynamically (*52*) or dynamically (*9*) coupled in other PDZ domains in the amino acid sequence (Figure 6A). Furthermore, we structurally align PSD-95 PDZ3 with AF-6 PDZ (Figure 6C) and hPTP1E PDZ2 with AF-6 PDZ (Figure 6D). We also find that nearly all of these 12 residues are structurally close to the residues that were previously reported to be thermodynamically or dynamically coupled in other PDZ domains (Figure 6C,D). Therefore, the millisecond time scale dynamics in the weak saturation state may map a network in the AF-6 PDZ domain in which the energetic signals are transduced to distal regions in the protein.

Structural Response to Ligand Binding in Distal Surface 2. The region around the αA helix was named "distal surface 2" (Figure 6B) (*9*), where the PDZ domain of Par6 protein interacts with other proteins such as PALS1 (*56*) and Par3 (*57*). In the previous study of the allosteric transition in CRIB-PDZ of Par6 protein, the binding of Cdc42 at distal surface 2 of the Par6 PDZ domain caused conformational changes in the peptide binding pocket. In another analysis of the structure of the PDZ-C-terminal peptide complex, the authors found that changes in the protein structure around the αA helix were similar to that caused by the Cdc42 binding (*12*).

In the AF-6 PDZ domain, during titration with Bcr peptide, residues A45 and D46 of the αA helix exhibited obvious chemical shift changes, ~0.4−0.6 ppm in the ^{15}N dimension (Figure 1B) (*6*), and residues from αA also showed deviation between free and complex forms with a rmsd value of 1.13 Å (*8*). Though the residues of the αA helix are ~12 Å from the center of the βB strand, their dissociation constants are similar to those of the residues in the peptide binding groove (Table 1). It seems that the structure rearrangement of αA helix is caused by the interaction in the binding groove between the protein and the peptide, i.e., allostery.

The residues around distal surface 2 had no chemical exchange in the free state (Figure 3A) and exhibited no chemical exchange during Bcr peptide binding except for residue A44 (Figure 3). Similar results were also obtained from the backbone picosecond to nanosecond dynamics measurements in free and complex states of that PDZ domain (*8*) and implied that the allosteric process in distal surface 2 of the AF-6 PDZ domain might be mainly intermediated by structure changes.

The allosteric processes were proposed not to be intrinsic to the PDZ family, and the interaction networks may be functionally exploited only in some cases (*58*). Comparison of our results with the results for other PDZ domains was consistent with that proposition. For example, like our result with the AF-6 PDZ domain, a similar allosteric process (structure rearrangement around αA helix) was observed for the Par6 PDZ domain upon peptide binding (*12*), whereas that allosteric effect was not observed for hPTP1E PDZ2 (*59*) or PSD-95 PDZ3 (*60*).

Dynamical Response to Ligand Binding in Distal Surface 1. When the PDZ domain was saturated, five residues distal from the peptide binding groove exhibited millisecond motions (N15, R63, L65, L68, and R79). Considering that the free PDZ domain was less than 1% when the PDZ domain was saturated, those motions should be intramolecu-

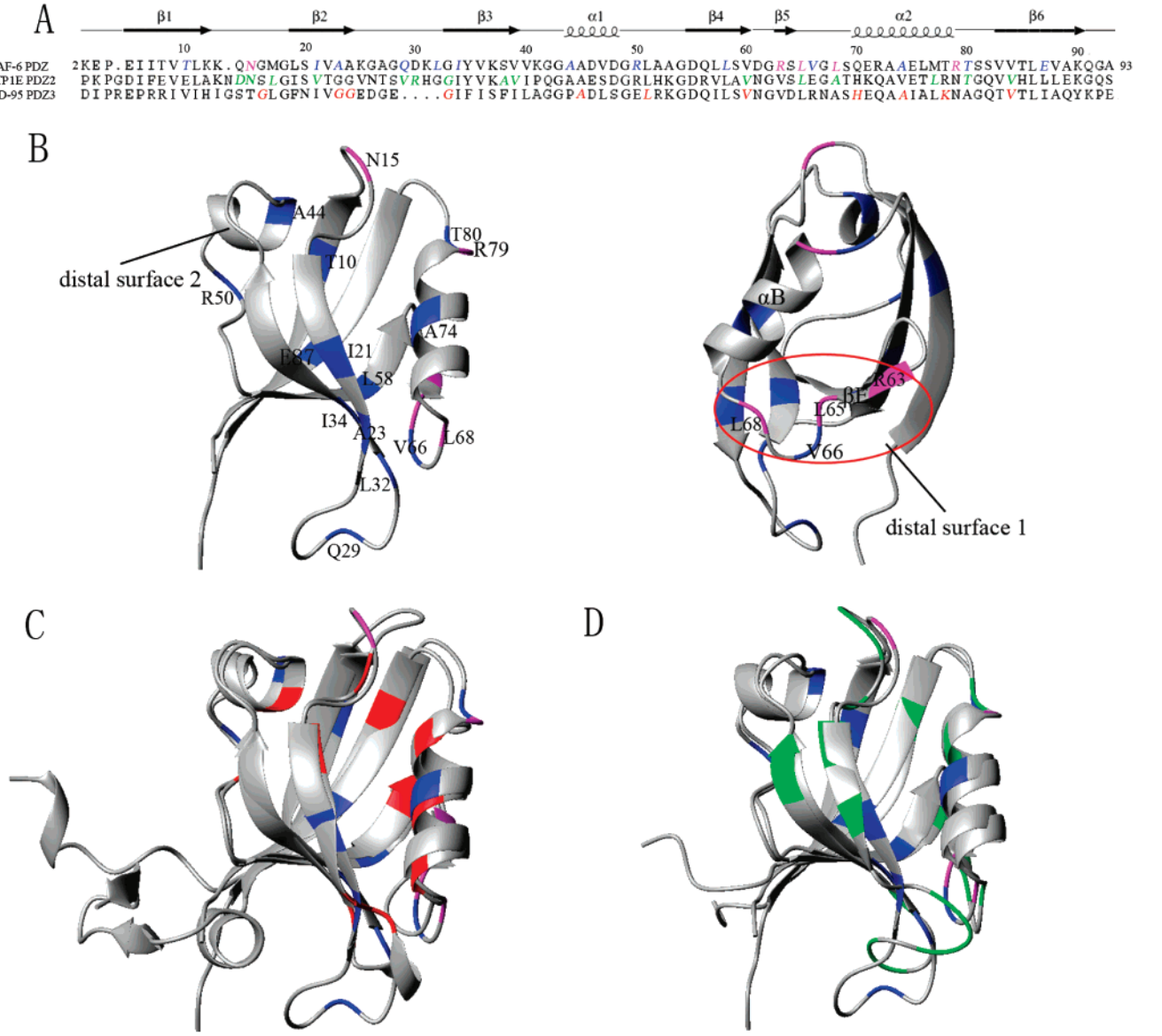

FIGURE 6: (A) Amino acid sequence alignment of three PDZ domains: AF-6 PDZ, hPTP1E PDZ2, and PSD-95 PDZ3 (Protein Data Bank entries 1T2M, 1D5G, and 1TP3). Residues that exhibit interesting millisecond behaviors are colored blue or magenta (as mentioned for panel B) in AF-6 PDZ. Dynamically coupled residues identified previously are colored green in hPTP1E PDZ2 (*9*), and thermodynamically coupled residues identified previously are colored red in PSD-95 PDZ3 (*52*). (B) Different views of the AF-6 PDZ domain. Residues (colored blue) for which millisecond dynamics change significantly ($|\Delta R_{ex}| > 1$) after the addition of a small amount of peptide and residues (colored magenta) that exhibit intramolecular millisecond motions in the complex state. (C and D) Structural alignment of AF-6 PDZ with PSD-95 PDZ3 (C) and structural alignment of AF-6 PDZ with hPTP1E PDZ2 (D). Residues that exhibit interesting millisecond behaviors are colored blue or magenta as mentioned for panel B in AF-6 PDZ. Thermodynamically coupled residues are colored red in PSD-95 PDZ3 (C) (*52*), and dynamically coupled residues are colored green in hPTP1E PDZ2 (D) (*9*).

lar dynamics of complex PDZ in nature. These residues also had obvious correlations with those that were identified previously to be thermodynamically (*52*) or dynamically (*9*) linked to peptide binding (Figure 6). Two of those residues are located at the loop connecting βE and αB, and one is located at βE. That surface is another potential protein−protein interaction surface of the AF-6 PDZ domain ["distal surface 1" (Figure 6B)] (*9*). In the NMR studies of PDZ7 from GRIP1, a Ras guanine nucleotide exchange factor, GRASP-1, that hydrophobic surface was the binding site for PDZ7 (*61*). During the titration with Bcr peptide, residues in distal surface 1 showed little chemical shift perturbation [<0.05 ppm in the ^{15}N dimension (Figure 1B)], and the structures of the AF-6 PDZ domain in free and complex forms exhibited nearly no difference around βE (*8*).

In contrast, the millisecond dynamics in distal surface 1 changed obviously during peptide binding. Whereas residues around the βE strand exhibited no millisecond dynamics in the free or weak saturation state, when the AF-6 PDZ domain was saturated, residues R63 and L65 exhibited millisecond motions (Figure 3 and Table 4). As shown in Figure 6B, three residues (R63, L65, and L68) exhibited intramolecular millisecond dynamics on distal surface 1, and some other residues, such as V66, S69, and A73, also exhibited changes in millisecond dynamics during peptide binding (Tables 2−4).

In the studies of side chain picosecond to nanosecond dynamics for the hPTP1E PDZ2 domain, residues in distal surface 1 had significant changes in dynamic parameters S_{axis}^2 and τ_e upon ligand binding or point mutation (*9*, *11*).

Recently, Popovych and his co-workers (*31*) proved that the allostery could be driven purely by the dynamics, and in their experiments, the microsecond to millisecond dynamics also provided a means of propagating the allosteric signal to the distal site in the absence of structural changes. Thus, the changes in millisecond dynamics in distal surface 1 of the AF-6 PDZ domain may also be the result of allosteric signal transmission. That allosteric process may be mainly driven by dynamics since the structure of distal surface 1 changed little during that process (*8*).

In summary, we compared the structures of the AF-6 PDZ domain in free and complex forms (*8*) and probed the millisecond time scale dynamics of the AF-6 PDZ domain in response to Bcr peptides binding using relaxation dispersion experiments. Large conformational switching on the millisecond time scale is not observed. The millisecond dynamics of the AF-6 PDZ domain in the weak saturation state may represent a network for allosteric signal transmission throughout the protein, and the process of perturbation propagation can be decomposed into smaller events on the millisecond time scale. When the AF-6 PDZ domain is complexed with Bcr peptide, some residues in distal surface 1 exhibit intramolecular motions. Thus, the millisecond dynamics still play an important role in this allosteric process and provide a mechanism for the transmission of allosteric signals throughout the AF-6 PDZ domain just as picosecond to nanosecond dynamics do in hPTP1E PDZ2 (*9*). Interestingly, in the two distal surfaces, the allostery process is driven mainly by structure or dynamics. Although there is no experimental evidence of the actual functional allostery in the system of the AF-6 PDZ domain, our works may provide a basis for further studies aimed at addressing this complicated issue.

ACKNOWLEDGMENT

We thank Dr. Hy Zhou for providing the recombinant plasmid of the human AF-6 PDZ domain. We thank Mr. Zf Luo for technical support of ITC. We thank Dr. F. Delaglio and Prof. A. Bax for providing NMRPipe, Prof. T. D. Goddard and Prof. D. G. Kneller for providing Sparky, and Dr. R. Koradi and Prof. K. Wüthrich for providing MOLMOL. We thank Dr. U. L. Günther for providing the NMRKIN.

SUPPORTING INFORMATION AVAILABLE

Thermodynamic analysis of the interaction between the AF-6 PDZ domain and Bcr peptide by isothermal titration calorimetry (Figure S1), results of standard T_2 relaxation experiments with the AF-6 PDZ domain at 1 and 0.5 mM (Figure S2), and line shapes of residues G18 and A23 of the AF-6 PDZ domain during Bcr peptide titration (Figure S3). This material is available free of charge via the Internet at http://pubs.acs.org.

REFERENCES

1. Morais Cabral, J. H., Petosa, C., Sutcliffe, M. J., Raza, S., Byron, O., Poy, F., Marfatia, S. M., Chishti, A. H., and Liddington, R. C. (1996) Crystal structure of a PDZ domain, *Nature 382*, 649−652.
2. Hung, A. Y., and Sheng, M. (2002) PDZ domains: Structural modules for protein complex assembly, *J. Biol. Chem. 277*, 5699−5702.
3. Hillier, B. J., Christopherson, K. S., Prehoda, K. E., Bredt, D. S., and Lim, W. A. (1999) Unexpected modes of PDZ domain scaffolding revealed by structure of nNOS-syntrophin complex, *Science 284*, 812−815.
4. Su, L., Hattori, M., Moriyama, M., Murata, N., Harazaki, M., Kaibuchi, K., and Minato, N. (2003) AF-6 controls integrin-mediated cell adhesion by regulating Rap1 activation through the specific recruitment of Rap1GTP and SPA-1, *J. Biol. Chem. 278*, 15232−15238.
5. Ikeda, W., Nakanishi, H., Miyoshi, J., Mandai, K., Ishizaki, H., Tanaka, M., Togawa, A., Takahashi, K., Nishioka, H., Yoshida, H., Mizoguchi, A., Nishikawa, S., and Takai, Y. (1999) Afadin: A key molecule essential for structural organization of cell-cell junctions of polarized epithelia during embryogenesis, *J. Cell Biol. 146*, 1117−1132.
6. Zhou, H., Xu, Y., Yang, Y., Huang, A., Wu, J., and Shi, Y. (2005) Solution structure of AF-6 PDZ domain and its interaction with the C-terminal peptides from Neurexin and Bcr, *J. Biol. Chem. 280*, 13841−13847.
7. Radziwill, G., Erdmann, R. A., Margelisch, U., and Moelling, K. (2003) The Bcr kinase downregulates Ras signaling by phosphorylating AF-6 and binding to its PDZ domain, *Mol. Cell. Biol. 23*, 4663−4672.
8. Chen, Q., Niu, X., Xu, Y., Wu, J., and Shi, Y. (2007) Solution Structure and Backbone Dynamics of AF-6 PDZ domain/Bcr Peptide Complex, *Protein Sci. 16*, 1053−1062.
9. Fuentes, E. J., Der, C. J., and Lee, A. L. (2004) Ligand-dependent dynamics and intramolecular signaling in a PDZ domain, *J. Mol. Biol. 335*, 1105−1115.
10. Kern, D., and Zuiderweg, E. R. (2003) The role of dynamics in allosteric regulation, *Curr. Opin. Struct. Biol. 13*, 748−757.
11. Fuentes, E. J., Gilmore, S. A., Mauldin, R. V., and Lee, A. L. (2006) Evaluation of Energetic and Dynamic Coupling Networks in a PDZ Domain Protein, *J. Mol. Biol. 364*, 337−351.
12. Peterson, F. C., Penkert, R. R., Volkman, B. F., and Prehoda, K. E. (2004) Cdc42 regulates the Par-6 PDZ domain through an allosteric CRIB-PDZ transition, *Mol. Cell 13*, 665−676.
13. Kovrigin, E. L., and Loria, J. P. (2006) Enzyme dynamics along the reaction coordinate: Critical role of a conserved residue, *Biochemistry 45*, 2636−2647.
14. Ding, Z., Lee, G. I., Liang, X., Gallazzi, F., Arunima, A., and Van Doren, S. R. (2005) PhosphoThr peptide binding globally rigidifies much of the FHA domain from *Arabidopsis* receptor kinase-associated protein phosphatase, *Biochemistry 44*, 10119−10134.
15. Yang, D., and Kay, L. E. (1996) Contributions to conformational entropy arising from bond vector fluctuations measured from NMR-derived order parameters: Application to protein folding, *J. Mol. Biol. 263*, 369−382.
16. Li, Z., Raychaudhuri, S., and Wand, A. J. (1996) Insights into the local residual entropy of proteins provided by NMR relaxation, *Protein Sci. 5*, 2647−2650.
17. Akke, M., Skelton, N. J., Kordel, J., Palmer, A. G., III, and Chazin, W. J. (1993) Effects of ion binding on the backbone dynamics of calbindin D9k determined by ^{15}N NMR relaxation, *Biochemistry 32*, 9832−9844.
18. Tollinger, M., Skrynnikov, N. R., Mulder, F. A. A., Forman-Kay, J. D., and Kay, L. E. (2001) Slow dynamics in folded and unfolded states of an SH3 domain, *J. Am. Chem. Soc. 123*, 11341−11352.
19. Palmer, A. G., III, Kroenke, C. D., and Loria, J. P. (2001) Nuclear magnetic resonance methods for quantifying microsecond-to-millisecond motions in biological macromolecules, *Methods Enzymol. 339*, 204−238.
20. Eisenmesser, E. Z., Bosco, D. A., Akke, M., and Kern, D. (2002) Enzyme dynamics during catalysis, *Science 295*, 1520−1523.
21. Eisenmesser, E. Z., Millet, O., Labeikovsky, W., Korzhnev, D. M., Wolf-Watz, M., Bosco, D. A., Skalicky, J. J., Kay, L. E., and Kern, D. (2005) Intrinsic dynamics of an enzyme underlies catalysis, *Nature 438*, 117−121.
22. Cole, R., and Loria, J. P. (2002) Evidence for flexibility in the function of ribonuclease A, *Biochemistry 41*, 6072−6081.
23. Beach, H., Cole, R., Gill, M. L., and Loria, J. P. (2005) Conservation of us-ms enzyme motions in the apo- and substrate-mimicked state, *J. Am. Chem. Soc. 127*, 9167−9176.
24. Mulder, F. A., Mittermaier, A., Hon, B., Dahlquist, F. W., and Kay, L. E. (2001) Studying excited states of proteins by NMR spectroscopy, *Nat. Struct. Biol. 8*, 932−935.
25. Grey, M. J., Wang, C., and Palmer, A. G., III (2003) Disulfide bond isomerization in basic pancreatic trypsin inhibitor: Multisite

chemical exchange quantified by CPMG relaxation dispersion and chemical shift modeling, *J. Am. Chem. Soc. 125*, 14324−14335.
26. Korzhnev, D. M., Salvatella, X., Vendruscolo, M., Di Nardo, A. A., Davidson, A. R., Dobson, C. M., and Kay, L. E. (2004) Low-populated folding intermediates of Fyn SH3 characterized by relaxation dispersion NMR, *Nature 430*, 586−590.
27. Hill, R. B., Bracken, C., DeGrado, W. F., and Palmer, A. G. (2000) Molecular motions and protein folding: Characterization of the backbone dynamics and folding equilibrium of alpha D-2 using C-13 NMR spin relaxation, *J. Am. Chem. Soc. 122*, 11610−11619.
28. Yao, S., Headey, S. J., Keizer, D. W., Bach, L. A., and Norton, R. S. (2004) C-Terminal domain of insulin-like growth factor (IGF) binding protein 6: Conformational exchange and its correlation with IGF-II binding, *Biochemistry 43*, 11187−11195.
29. Mittag, T., Schaffhausen, B., and Gunther, U. L. (2003) Direct observation of protein−ligand interaction kinetics, *Biochemistry 42*, 11128−11136.
30. Stevens, S. Y., Sanker, S., Kent, C., and Zuiderweg, E. R. (2001) Delineation of the allosteric mechanism of a cytidylyltransferase exhibiting negative cooperativity, *Nat. Struct. Biol. 8*, 947−952.
31. Popovych, N., Sun, S., Ebright, R. H., and Kalodimos, C. G. (2006) Dynamically driven protein allostery, *Nat. Struct. Mol. Biol. 13*, 831−838.
32. Millet, O., Loria, J. P., Kroenke, C. D., Pons, M., and Palmer, A. G. (2000) The static magnetic field dependence of chemical exchange linebroadening defines the NMR chemical shift time scale, *J. Am. Chem. Soc. 122*, 2867−2877.
33. Lian, L. Y., Barsukov, I. L., Sutcliffe, M. J., Sze, K. H., and Roberts, G. C. (1994) Protein-ligand interactions: Exchange processes and determination of ligand conformation and protein-ligand contacts, *Methods Enzymol. 239*, 657−700.
34. Liu, D., Prasad, R., Wilson, S. H., DeRose, E. F., and Mullen, G. P. (1996) Three-dimensional solution structure of the N-terminal domain of DNA polymerase β and mapping of the ssDNA interaction interface, *Biochemistry 35*, 6188−6200.
35. Hu, H. Y., Horton, J. K., Gryk, M. R., Prasad, R., Naron, J. M., Sun, D. A., Hecht, S. M., Wilson, S. H., and Mullen, G. P. (2004) Identification of small molecule synthetic inhibitors of DNA polymerase β by NMR chemical shift mapping, *J. Biol. Chem. 279*, 39736−39744.
36. Carver, J. P., and Richards, R. E. (1972) A general two-site solution for the chemical exchange produced dependence of T2 upon the Carr-Purcell pulse separation, *J. Magn. Reson. 6*, 89−105.
37. Jen, J. (1978) Chemical exchange and NMR T2 relaxation: The multisite case, *J. Magn. Reson. 30*, 111−128.
38. Davis, D. G., Perlman, M. E., and London, R. E. (1994) Direct Measurements of the Dissociation-Rate Constant for Inhibitor-Enzyme Complexes Via the T-1-Rho and T-2 (Cpmg) Methods, *J. Magn. Reson., Ser. B 104*, 266−275.
39. Leavitt, S., and Freire, E. (2001) Direct measurement of protein binding energetics by isothermal titration calorimetry, *Curr. Opin. Struct. Biol. 11*, 560−566.
40. Farrow, N. A., Muhandiram, R., Singer, A. U., Pascal, S. M., Kay, C. M., Gish, G., Shoelson, S. E., Pawson, T., Formankay, J. D., and Kay, L. E. (1994) Backbone Dynamics of a Free and a Phosphopeptide-Complexed Src Homology-2 Domain Studied by N-15 Nmr Relaxation, *Biochemistry 33*, 5984−6003.
41. Gunther, U., Mittag, T., and Schaffhausen, B. (2002) Probing Src homology 2 domain ligand interactions by differential line broadening, *Biochemistry 41*, 11658−11669.
42. Mittag, T., Schaffhausen, B., and Gunther, U. L. (2004) Tracing kinetic intermediates during ligand binding, *J. Am. Chem. Soc. 126*, 9017−9023.
43. Gunasekaran, K., Ma, B., and Nussinov, R. (2004) Is allostery an intrinsic property of all dynamic proteins? *Proteins 57*, 433−443.
44. Monod, J., Wyman, J., and Changeux, J. P. (1965) On the Nature of Allosteric Transitions: A Plausible Model, *J. Mol. Biol. 12*, 88−118.
45. Changeux, J. P., and Edelstein, S. J. (2005) Allosteric mechanisms of signal transduction, *Science 308*, 1424−1428.
46. Swain, J. F., and Gierasch, L. M. (2006) The changing landscape of protein allostery, *Curr. Opin. Struct. Biol. 16*, 102−108.
47. Perutz, M. F. (1970) Stereochemistry of cooperative effects in haemoglobin, *Nature 228*, 726−739.
48. Lipscomb, W. N. (1994) Aspartate transcarbamylase from *Escherichia coli*: Activity and regulation, *Adv. Enzymol. Relat. Areas Mol. Biol. 68*, 67−151.
49. Ascenzi, P., Bocedi, A., Bolli, A., Fasano, M., Notari, S., and Polticelli, F. (2005) Allosteric modulation of monomeric proteins, *Biochem. Mol. Biol. Educ. 33*, 169−176.
50. Cooper, A., and Dryden, D. T. F. (1984) Allostery without Conformational Change: A Plausible Model, *Eur. Biophys. J. 11*, 103−109.
51. Falke, J. J. (2002) Enzymology. A moving story, *Science 295*, 1480−1481.
52. Lockless, S. W., and Ranganathan, R. (1999) Evolutionarily conserved pathways of energetic connectivity in protein families, *Science 286*, 295−299.
53. Feher, V. A., and Cavanagh, J. (1999) Millisecond-timescale motions contribute to the function of the bacterial response regulator protein Spo0F, *Nature 400*, 289−293.
54. Duggan, B. M., Dyson, H. J., and Wright, P. E. (1999) Inherent flexibility in a potent inhibitor of blood coagulation, recombinant nematode anticoagulant protein c2, *Eur. J. Biochem. 265*, 539−548.
55. Volkman, B. F., Lipson, D., Wemmer, D. E., and Kern, D. (2001) Two-state allosteric behavior in a single-domain signaling protein, *Science 291*, 2429−2433.
56. Hurd, T. W., Gao, L., Roh, M. H., Macara, I. G., and Margolis, B. (2003) Direct interaction of two polarity complexes implicated in epithelial tight junction assembly, *Nat. Cell Biol. 5*, 137−142.
57. Joberty, G., Petersen, C., Gao, L., and Macara, I. G. (2000) The cell-polarity protein Par6 links Par3 and atypical protein kinase C to Cdc42, *Nat. Cell Biol. 2*, 531−539.
58. Gianni, S., Walma, T., Arcovito, A., Calosci, N., Bellelli, A., Engstrom, A., Travaglini-Allocatelli, C., Brunori, M., Jemth, P., and Vuister, G. W. (2006) Demonstration of long-range interactions in a PDZ domain by NMR, kinetics, and protein engineering, *Structure 14*, 1801−1809.
59. Kozlov, G., Banville, D., Gehring, K., and Ekiel, I. (2002) Solution structure of the PDZ2 domain from cytosolic human phosphatase hPTP1E complexed with a peptide reveals contribution of the β2-β3 loop to PDZ domain-ligand interactions, *J. Mol. Biol. 320*, 813−820.
60. Doyle, D. A., Lee, A., Lewis, J., Kim, E., Sheng, M., and MacKinnon, R. (1996) Crystal structures of a complexed and peptide-free membrane protein-binding domain: Molecular basis of peptide recognition by PDZ, *Cell 85*, 1067−1076.
61. Feng, W., Fan, J. S., Jiang, M., Shi, Y. W., and Zhang, M. (2002) PDZ7 of glutamate receptor interacting protein binds to its target via a novel hydrophobic surface area, *J. Biol. Chem. 277*, 41140−41146.

BI701303P